Front. Chem. Sci. Eng. 2019, 13(3): 475–484
https://doi.org/10.1007/s11705-019-1809-0

RESEARCH ARTICLE

A non-lithographic plasma nanoassembly technology for polymeric nanodot and silicon nanopillar fabrication

Athanasios Smyrnakis (✉)[1], Angelos Zeniou[1,2], Kamil Awsiuk[3], Vassilios Constantoudis[1], Evangelos Gogolides[1]

1 Institute of Nanoscience & Nanotechnology, NCSR "Demokritos", Ag. Paraskevi, 15341 Attica, Greece
2 Department of Physics, University of Patras, 26504 Patras, Greece
3 M. Smoluchowski Institute of Physics, Jagiellonian University, 30-348 Krakow, Poland

© Higher Education Press and Springer-Verlag GmbH Germany, part of Springer Nature 2019

Abstract In this work, we present plasma etching alone as a directed assembly method to both create the nanodot pattern on an etched polymeric (PMMA) film and transfer it to a silicon substrate for the fabrication of silicon nanopillars or cone-like nanostructuring. By using a shield to control sputtering from inside the plasma reactor, the size and shape of the resulting nanodots can be better controlled by varying plasma parameters as the bias power. The effect of the shield on inhibitor deposition on the etched surfaces was investigated by time-of-flight secondary ion mass spectroscopy (ToF-SIMS) measurements. The fabrication of quasi-ordered PMMA nanodots of a diameter of 25 nm and period of 54 nm is demonstrated. Pattern transfer to the silicon substrate using the same plasma reactor was performed in two ways: (a) a mixed fluorine-fluorocarbon-oxygen nanoscale etch plasma process was employed to fabricate silicon nanopillars with a diameter of 25 nm and an aspect ratio of 5.6, which show the same periodicity as the nanodot pattern, and (b) high etch rate cryogenic plasma process was used for pattern transfer. The result is the nanostructuring of Si by high aspect ratio nanotip or nanocone-like features that show excellent antireflective properties.

Keywords plasma, nanoassembly, etching, nanodots, nanopillars, nanofabrication

1 Introduction

Etching roughness is usually considered as an unwanted issue in plasma processing. However, there are cases, where plasma induced roughness is beneficial and may result in the fabrication of ordered nanofeatures (dots, pillars, wires) [1], which is essential in many technological fields, due to a wide variety of potential applications. Plasma etching is mainly used to transfer patterns under the necessary requirement of having an initial etching mask on the substrate. These nanopatterns can be fabricated either by lithographic techniques such as optical lithography [2], extreme ultra-violet lithography [3], e-beam lithography [4], and nanoimprint lithography [5,6], or by self-assembly techniques such as colloidal particle self-assembly (also known as colloidal or nanosphere lithography) [7–9] and block copolymer [10,11]. It is evident that the nanopatterning step requires the use of specialized materials (photopolymers, block copolymers or colloidal spheres), or lithography processes with inaccessible equipment costs, or relatively complex processes that cannot be easily applied to large surfaces.

Using plasma etching alone as a self-assembly method to fabricate a nanopattern on a non-specialized, inexpensive and commercial polymer, and then transfer it to a subsequent layer in the same plasma reactor, the overall fabrication cost and time would be significantly decreased in a simplified nanofabrication process. There are several works demonstrated plasma as a process to assemble nanodots, nanotips or nanopillars without the use of lithography, based on the formation and random deposition of etch inhibitors on the surface during the etching process [12–16]. Alternative non-lithographic directed assembly nanofabrication processes also include ion-beam nanopatterning [17–19] that makes use of high energy ion beams to nanostructure hard substrates such as Si, InP.

Recently, we demonstrated plasma etching as a low-cost non-lithographic process, to direct the assembly of sub-50nm periodic dots on polymeric surfaces or films, such as PMMA [20,21]. These first efforts of plasma directed nanoassembly in the subtractive (etching) mode have limited process window as discussed by Kontziampasis et

Received September 1, 2018; accepted December 20, 2018

E-mail: a.smyrnakis@inn.demokritos.gr

al. [22], as application of bias voltage leads to loss of periodicity and growth of grass-like nanostructures. In addition, the nanodots are of low height, limiting their ability for pattern transfer to other substrates. Here, we establish subtractive plasma nanoassembly as a robust method for nanodot formation, demonstrating a large process window and a threefold increase of the nanodot height allowing facile pattern transfer to silicon or other substrates.

2 Experimental

Poly(methyl methacrylate) (PMMA, M_w = 120 k) dissolved in propylene glycol methyl ether acetate solution was used to fabricate thin polymeric films on silicon wafers by spin coating. Different film thicknesses range from 300 to 1600 nm were used by varying the solution concentration and spin coating speed. After spin coating, PMMA films were baked at 150°C for 90 min on a hotplate.

Plasma etching experiments were performed in a helicon antenna type, high density plasma tool (MET system, Adixen working in inductive mode). Oxygen gas at pressure of 0.75 Pa was used to etch the PMMA samples. Source power was 1900 W, while bias power from 0 to 250 W was tested. The O_2 flow was 100 sccm and the electrode temperature was 55°C. Samples of PMMA film on silicon were glued on a 4-inch silicon wafer acting as a carrier wafer to transfer the samples into the reactor chamber. Helium backside pressure enhances the thermal contact between the substrate and the electrode and assures thermal uniformity.

Si plasma etching was employed to transfer the pattern of the nanodots to silicon. Two different plasma processes were tested using the same plasma reactor. First, a mixed fluorine-fluorocarbon-oxygen nanoscale etch plasma process was used. It is a room temperature anisotropic process which forms a polymeric passivation layer. The source power is 1800 W and the bias generator power 65 W (this corresponds to −60–70 V bias voltage). The gas flows were 35, 85, and 30 sccm for SF_6, C_4F_8, and O_2, respectively, at a pressure of 1.8 Pa. In addition, the cryogenic Si etching process is used under the following plasma conditions: source power 1000 W, bias power 35 W (corresponds to −55 V bias voltage), and gas mixture of 200 sccm of SF_6 and 50 sccm of O_2 at a pressure of 1.33 Pa. The temperature was kept at −105°C. In the case of silicon etching, samples were glued with thermal paste on Si carrier wafer covered with a thick SU-8 film.

The morphology of the plasma etched surfaces was characterized by scanning electron microscopy on a JSM 7401F instrument from Jeol. Top-down scanning electron microscopy (SEM) image analysis have been performed using the nanoTOPO-SEM™ software by Nanometrisis. From the image analysis we can extract the mean width and period (mean distance) of the nanodots, and also the nearest neighbor index (NNI). The NNI indicates the spatial distribution of the dots: regularly dispersed (ordered), randomly dispersed, or clustered. It is defined as $NNI = 2D\sqrt{N/A}$, where D is the average distance between each point and each nearest neighbor, N is the number of studied points, and A is the size of the studied area. NNI measures the spatial distribution from 0 (clustered pattern) to 1 (randomly dispersed pattern) to 2.15 (regularly dispersed/uniform pattern). The height of the nanostructures is measured from tilted SEM images. Also, atomic force microscope (AFM) measurements were done on a CP-II instrument from Veeco. Measurements were performed in tapping mode, with the use of PPP-NCHR-50 tips (tip radius < 7 nm).

Plasma etched PMMA surfaces were analyzed using a ToF-SIMS 5 (ION-TOF GmbH) instrument. Each sample was scanned over an area of 200 × 200 µm in four different non-overlapping spots. Primary ion beam (30 keV Bi_3^+) was used with dose density lower than 10^{12} ions/cm^2 to ensure static mode conditions. The intensities of the selected peaks from each spectrum were normalized to the total counts. Normalization was carried out separately for positive and negative ions.

The reflectance (total, specular and diffuse) of the nanostructured silicon surfaces was measured using a ThetaMetrisis FR-Reflection kit which includes an Ocean Optics ISP-50-GT Integrating Sphere coupled to an Ocean Optics QE65000-ABS UV-NIR Spectrometer. A high-reflectivity specular reflectance standard from Ocean Optics calibrated to a NIST master was used as a reference. Solar-weighted reflectance, R_W, was calculated over the wavelength range between 280 and 950 nm with a resolution of 1 nm. It is defined as: $R_W = \Sigma_i \rho(\lambda_i) * F(\lambda_i)$, where $\rho(\lambda_i)$ is the reflectance measured experimentally and $F(\lambda_i)$ is the weight factor of each wavelength ($\Sigma_i F(\lambda_i) = 1$) taken from the ASTM G173-03(2012) standard (Standard tables for reference solar spectral irradiances: direct mormal and hemispherical on 37° tilted surface, ASTM International) and normalized in the range 280−950 nm.

3 Results and discussion

3.1 Polymeric nanodots fabrication

Plasma etching has been demonstrated as a non-lithographic, fast, and low-cost process, to direct the assembly of sub-50 nm periodic dots on polymeric surfaces or films, such as PMMA [20,22]. To get ordered nanodots, no external bias power must be applied to the electrode; otherwise, random nanotexturing of the polymeric surface and growth of grass-like structures occurs [1]. The mechanism behind this spontaneous nanodot formation

has been proven to be the combined result of fast etching of the polymer and simultaneous deposition of sputtered material from the plasma reactor chamber [23,24]. In the plasma reactor (a schematic of the plasma reactor can be found elsewhere [1]), there are two main sources of sputtering: (a) the first is the reactor upper alumina tube (or dome) surrounded by the half-nagoya type antenna, around which sputtering occurs when plasma is on to accelerate ions towards the upper tube walls, and cannot be prevented by the reactor without any electrostatic shield; and (b) the second is the electrode and its clamping ring, also made from alumina. Under plasma conditions with only the antenna being powered and having a high potential but without bias voltage applied on the electrode (P_{bias} = 0 W), the sputtered upper tube at the position of the antenna is the main source of inhibitors. The incident ion energy on the electrode surface is equal to the plasma potential (10–20 V), which is too low to cause sputtering from the electrode. On the contrary, when bias power is applied to the electrode, incident ions are of high energy ($V_{\mathrm{bias}} > 100$ V), and the electrode becomes also a main source of inhibitors. To avoid such sputtering from the electrode/clamping ring, one can either increase the size of the sample surface to cover all the electrode, or reduce the electrode surface to the size of the largest sample (in both cases eliminating the clamping ring), or shield parts of the electrode surface/clamping ring from ions. Here, we follow the approach of shielding parts of the electrode/clamping ring using a custom made ground shield above it as described elsewhere [25].

ToF-SIMS was employed to study the surface composition of the etched PMMA samples, and determine the amount of sputtered inhibitors, in our case Al. PMMA samples were etched in O_2 plasma for 5 min under various bias power conditions (0, 50, 150, and 250 W) and different clamping ring condition, with or without the shield placed. Table 1 presents the bias voltage and etch rate for PMMA films under different bias power and electrode shielding conditions. The etch rates were determined by ellipsometry measurements after etching for 1 min. Under these conditions, no significant roughness was developed. However, even if we continue the measurement for longer time, the thickness versus time curve remains linear. We see that the shield causes significant increase in the bias voltage. The shielded clamping ring is now grounded, so plasma ions seem to focus on the sample area. This increase in the energy of the incident ions results also in the increase of the etch rate.

Figures 1(a–c) show the normalized intensity of aluminum (Al^+) and aluminum oxides (AlO^-, AlO_2^-), that were detected on the plasma-etched PMMA surfaces for different bias power, with or without the clamping ring shield. The untreated surface shows totally absence of Al, and little amount of Al and its oxides is present even for 0 W bias power, which can be attributed to the sputtering from the upper tube of the reactor that is not shielded. For the unshielded electrode, the amount of Al^+, AlO^- and AlO_2^- increases dramatically with the increase of the bias power. On the contrary, for the shielded electrode only a minimal increase is observed, even though the bias voltage (incident ion energy) is much higher as shown in Table 1. For the maximum bias power of 250 W, the amount of Al^+ is one order of magnitude lower compared to the unshielded case. Therefore, we can deduce that the shield cuts off completely the sputtering of inhibitors from the electrode's clamping ring, leaving only the inhibitors that come from the alumina upper tube. We also see that sputtering from the electrode prevails sputtering from the upper tube for an unshielded chamber.

The morphology of the plasma-etched surfaces was characterized by SEM. The AFM image of Fig. 2(a) shows the result of oxygen plasma etching of PMMA thin films for 2 min with 0 W bias power and no shield. Etching of the PMMA film has stopped before the nanodots reach the substrate, so the Si surface is not exposed. The height of these nanodots is ~15–20 nm as can be seen in the AFM line scan in the inset. The SEM image of Fig. 2(b) shows the result of etching for 2 min by applying 136 V bias voltage (corresponds to 250 W bias power) with the clamping ring being unshielded. The result is the formation of random texturing due to the large amount of etch inhibitors sputtered from the unshielded ring. The height of this roughness is on the order of 1 μm. In Fig. 2(c) we present the result after 2 min oxygen plasma etching of PMMA by applying 130 V voltage bias, but with the clamping ring being shielded. Under these bias and shield conditions, well-defined and uniform nanodots form, and are similar with the nanodots obtained in the absence of bias power and the shield (Fig. 2(a)) but are taller in height. We also see that the significant Al inhibitor flow reduction

Table 1 Bias voltage and PMMA etch rate in O_2 plasma as a function of the bias power for unshielded and shielded electrodes

Bias power /W	Bias voltage /V		PMMA etch rate /(μm·min^{-1})	
	Unshielded	Shielded	Unshielded	Shielded
0	10	8	0.37	0.44
50	22	133	0.90	1.30
150	88	262	1.07	2.00
250	136	348	1.57	2.50

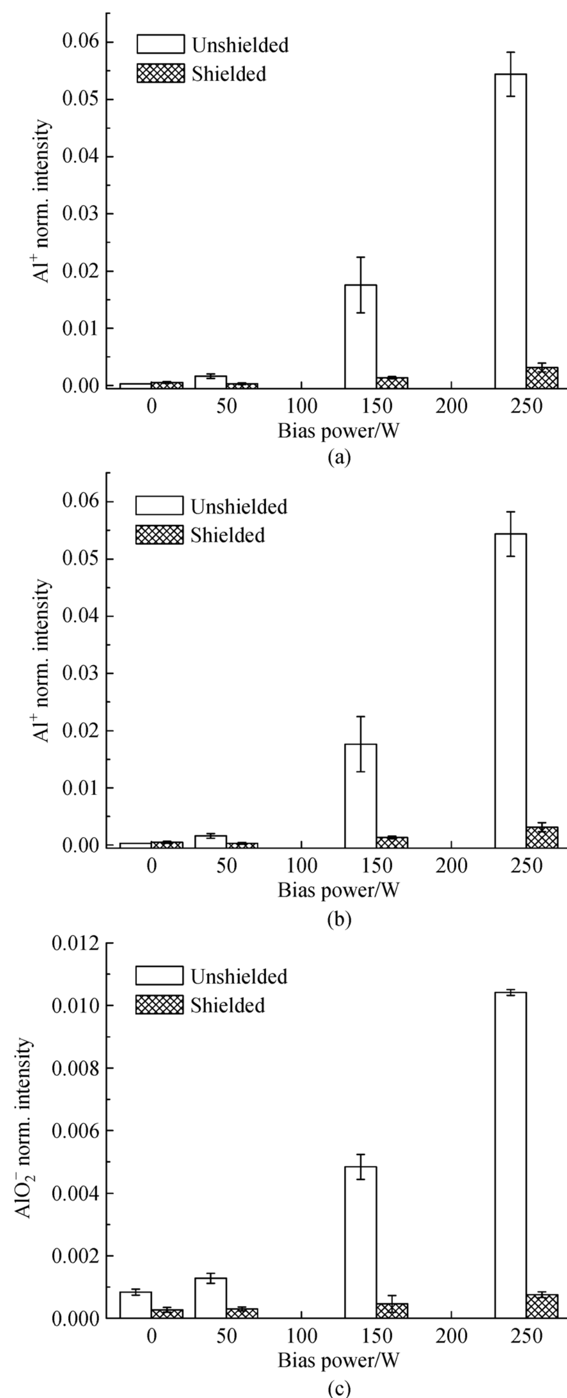

Fig. 1 ToF-SIMS measurements showing the amount (normalized peak intensity of the mass spectrum) of (a) aluminum (Al^+), (b), AlO^- , and (c) AlO_2^-, on PMMA surfaces etched in O_2 plasma for 5 min, under different bias power conditions, with or without the clamping ring shield

caused by the shield implies significant roughness reduction. Sputtering of inhibitors from the upper tube of the chamber is responsible for the nanodot formation of Fig. 2(c) because the shield prevents sputtering from the electrode. At the same time, the application of bias voltage of 130 V (corresponds to power 50 W) increases the etch rate of PMMA and etch selectivity to the hard inhibitors, making the nanodots taller. This is very important, as our goal is to use these nanodots as an etching mask to transfer the pattern to a subsequent silicon wafer.

Figure 3 shows top-down SEM images of plasma-etched PMMA films under different bias power (P_{bias}) conditions

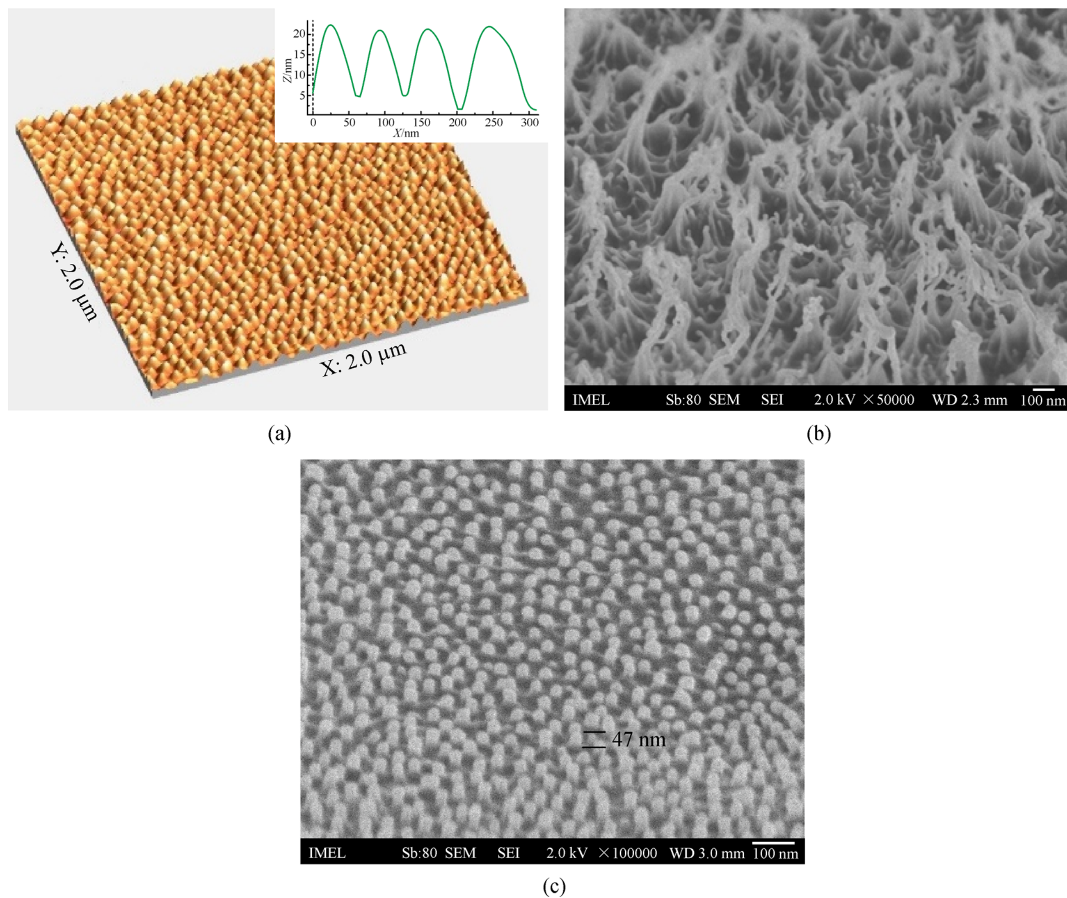

Fig. 2 (a) AFM image of PMMA surface (2 μm × 2 μm, 512 × 512 points) after 2 min O_2 plasma treatment using 0 W bias power and without the shield (inset: AFM line scan of the nanodots profile, and the nanodot height is ~15−20 nm; SEM images (tilted 45°) of PMMA surfaces etched in O_2 plasma for 2 min); (b) under 136 V bias voltage (250 W bias power) without the shield; (c) under 130 V bias voltage (50 W bias power) with the shield placed on the clamping ring of the electrode, and the nanodot height is ~47 nm. Notice the large process window for bias and the large height of the nanodots. Plasma conditions: antenna power 1900 W, O_2 flow 100 sccm at pressure of 0.75 Pa and temperature 15°C

and under different etching time conditions, to see the effect to the width, period and order of the nanodots. In all cases the clamping ring of the electrode remains shielded. These SEM images were analyzed using the nanoTOPO-SEM™ software from Nanometrisis [26].

As shown in Fig. 4, the mean width of the nanodots slightly increases with increasing time. For the case of 60 s, the mean width is identical (~25 nm) for the bias power of 50 and 100 W, and increases to ~29.5 nm at 150 W. The period of the nanodots increases when increasing the bias power and is 54 nm for P_{bias} = 50 W, 63 nm for P_{bias} = 100 W, and 93.5 nm for P_{bias} = 150 W. The period is not affected by the time for P_{bias} = 50 W, as it remains constant at 54 nm at 60, 90 and 120 s of etching. The height of the nanodots increases from 47 to 78 nm for P_{bias} equal to 50 and 100 W, respectively, and then decreases to 61 nm at the P_{bias} of 150 W. The nanostructures seem to melt and bend due to the significant increase of the bias voltage, which also increases the surface temperature. Concerning the arrangement of the nanodots, for the P_{bias} of 50 W the NNI takes values higher than 1.50 and it does not depend on the etching time. So the nanodots show a degree of periodicity and are quasi-order. Better order is achieved at the etching time of 30 s when bias power is 50 W, and NNI = 1.58. As the bias power increases, NNI decreases and therefore order is lost.

Figures 4(d) shows the circularly averaged Fourier Transform versus bias power, for the PMMA nanodots shown in Figs. 3(a–c). A steeper peak is an indication of better periodicity. Thus, we conclude that optimal organization is achieved for P_{bias} = 50 W. To summarize, we found that the mechanism behind the formation of ordered and quasi-ordered polymeric nanodots after O_2 treatment is the co-deposition of inhibitors due to sputtering from the upper alumina tube of the reactor chamber. On the other hand, the formation of high roughness on the surfaces is due to sputtering of inhibitors from the electrode clamping ring. The use of a shield on the

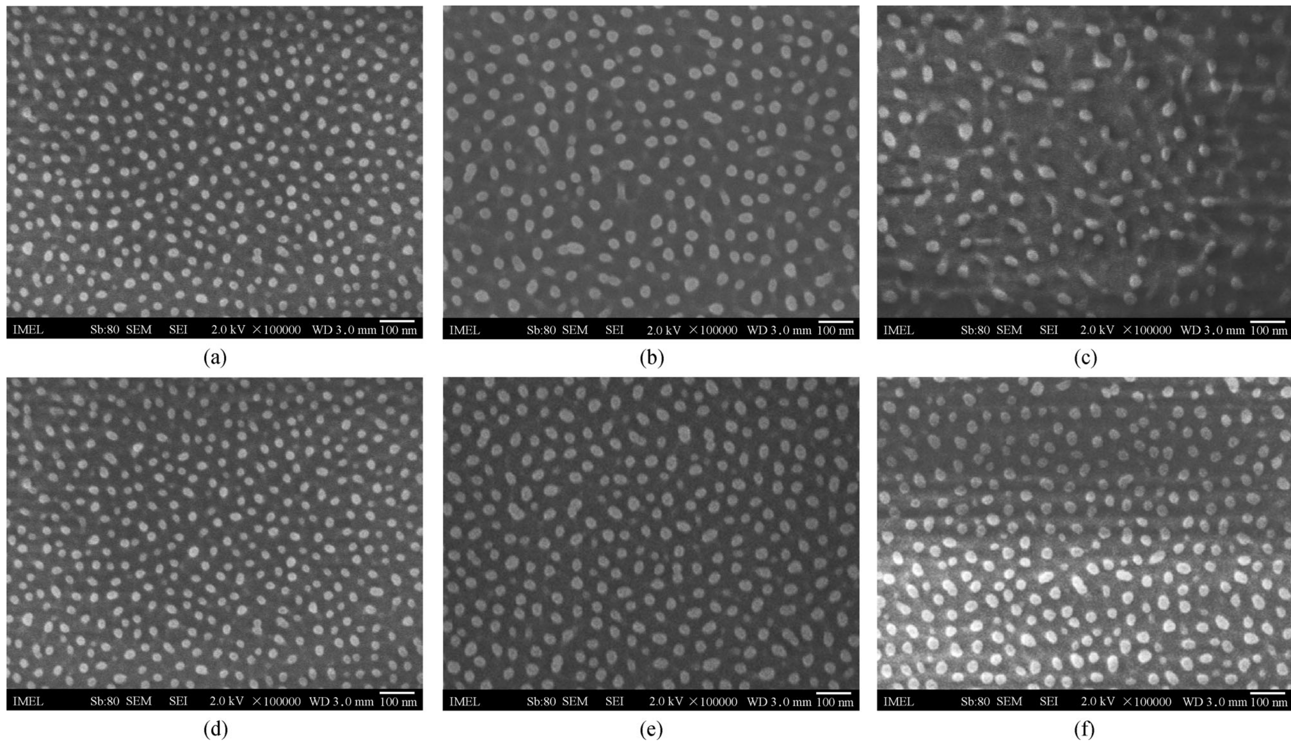

Fig. 3 Top-down SEM images of plasma-etched PMMA films under different bias power (P_{bias}) conditions and under different etching time conditions. The shield is applied on the electrode in all cases. Plasma conditions are (a) P_{bias} = 50 W, t = 60 s, (b) P_{bias} = 100 W, t = 60 s, (c) P_{bias} = 150 W, t = 60 s, (d) P_{bias} = 50 W, t = 30 s, (e) P_{bias} = 50 W, t = 90 s, and (f) P_{bias} = 50 W, t = 120 s

electrode helps to control and diminish sputtering from this ring. Therefore, bias power can be used to control the size, in terms of mean width and height, of the resulting nanodots.

3.2 Pattern transfer for Si nanopillar fabrication

The nanodots are formed on thin PMMA films and oxygen plasma etching stops when they reach the subsequent silicon layer. In this case, the nanodots can serve as an etching mask pattern, and subsequently we can transfer this pattern to Si using the same plasma reactor to fabricate silicon nanopillars. The exact time when the nanodots reach the silicon layer is controlled by *in situ* or *ex situ* spectroscopic ellipsometry, by which we monitor the remaining PMMA film thickness, and the etch rate. As there might be some variability in the etch rate of PMMA, monitoring of the etch rate is crucial. To take into account the presence of the nanodots on the surface, we use the Effective Medium Approximation in our model when fitting the Ψ, Δ signals of the ellipsometry measurement. The nanodot layer can be approached as the mixed PMMA/air material layer, which is on the top of a PMMA layer. Details about the use of spectroscopic ellipsometry in our etcher for monitoring of the film thickness versus etching time and surface roughness characterization can be found in our previous works [20,27]. Pattern transfer to the silicon substrate was performed in two ways using the same plasma reactor.

First, a mixed fluorine-fluorocarbon-oxygen nanoscale etch plasma process was used. It is a room temperature anisotropic process which forms a polymeric passivation layer (CO_xF_y). Etching and passivation of the sidewalls take place simultaneously. The etch rate of silicon is 240 nm/min, the etch rate of PMMA is 110 nm/min, resulting in an etch selectivity to PMMA of 2.4 ($S_{Si:PMMA}$). It is a mild process in terms of etch rate and selectivity, compared to other high etch rate DRIE processes such as the cryogenic process or the Bosch (gas alternating) process. However, the low selectivity can be beneficial as the process will etch fast any residual PMMA layer (few nanometers) among the nanodots, to expose the Si surface to the plasma, and start Si etching without changing the shape of the nanodots. For the pattern transfer experiments, we started from 1.7 μm PMMA film on Si. PMMA was etched in O_2 plasma for 75 s in order for the nanodots to reach the substrate. Plasma conditions were: Power 1900 W, bias power 50 W (133 V), 100 sccm O_2 at 0.75 Pa.

Figures 5(a–b) show SEM images (tilted at 45° and top-down, respectively) of Si nanopillars etched by the room temperature mixed fluorine-fluorocarbon-oxygen plasma process for 45 s, using as a mask for the PMMA nanodots.

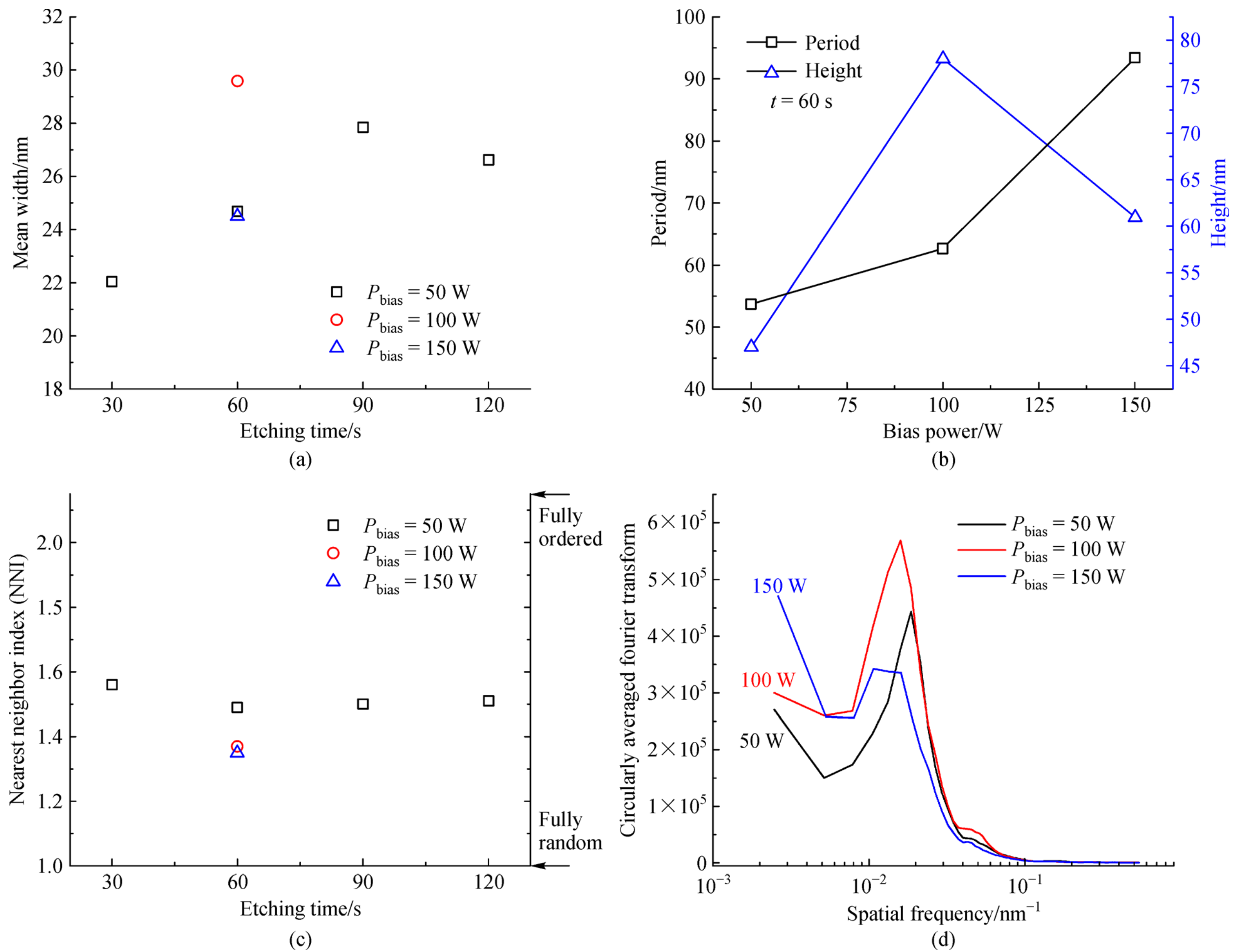

Fig. 4 (a) Mean width of the PMMA nanodots versus etching time and bias power, (b) period and height of the nanodots versus bias power, (c) NNI of the nanodots versus etching time and bias power, and (d) circularly averaged Fourier Transform versus the bias power. All values extracted by the SEM image analysis shown in Fig. 3 using the nanoTOPO-SEM™ software from Nanometrisis

SEM images were analyzed by the nanoTOPO-SEM™ software. The mean diameter of the Si nanopillars is 25.4±5.0 nm, the period is 62 nm and the height is 140 nm leading to an aspect ratio (AR, meaning the ratio of the mean diameter to the height of the pillars) of 5.6. This is the maximum AR that can be achieved using the mixed process as at the etching time of 45 s, the nanodot mask pattern is etched completely. The NNI of the Si nanopillars is 1.60, almost equal to the NNI of the nanodots, revealing that the same pattern is preserved after the pattern transfer. In Fig. 5(c), the circularly average Fourier Transform of the nanostructures before and after the pattern transfer is presented. Both patterns show a characteristic peak, and as a consequence the same order remains after the pattern transfer to Si.

In addition, the cryogenic Si etching process is used for the pattern transfer. It is a clean anisotropic process that makes use of a SF_6/O_2 gas mixture at cryogenic temperature ($T < -100$°C) [28–30]. The etch rate of silicon for the cryogenic process is 2 μm/min, and the etch rate of PMMA is 44 nm/min, resulting in an etch selectivity of Si to PMMA that is $S_{Si:PMMA}$ = 45. The same PMMA nanodot pattern described for the room-temperature process was also used for the pattern transfer experiments with the cryogenic process. We note that in all pattern transfer experiments a reference sample was also used which consist of a bare Si surface that also has some lines patterned on it by optical lithography. The role of the reference sample is to identify if the cryogenic etching operates in anisotropic mode, which means that there is no formation of “black silicon” [31,32] on the bare areas due to overpassivation, and the etched lines show vertical sidewalls. Also, from the reference sample we extract the etch rate of silicon.

Figures 6(a) and 6(b) show SEM images of the silicon nanostructured surface after cryogenic etching for 25 and 85 s, respectively. The height of these structures varies from a few tens of nanometers at 25 s, to reach a height of

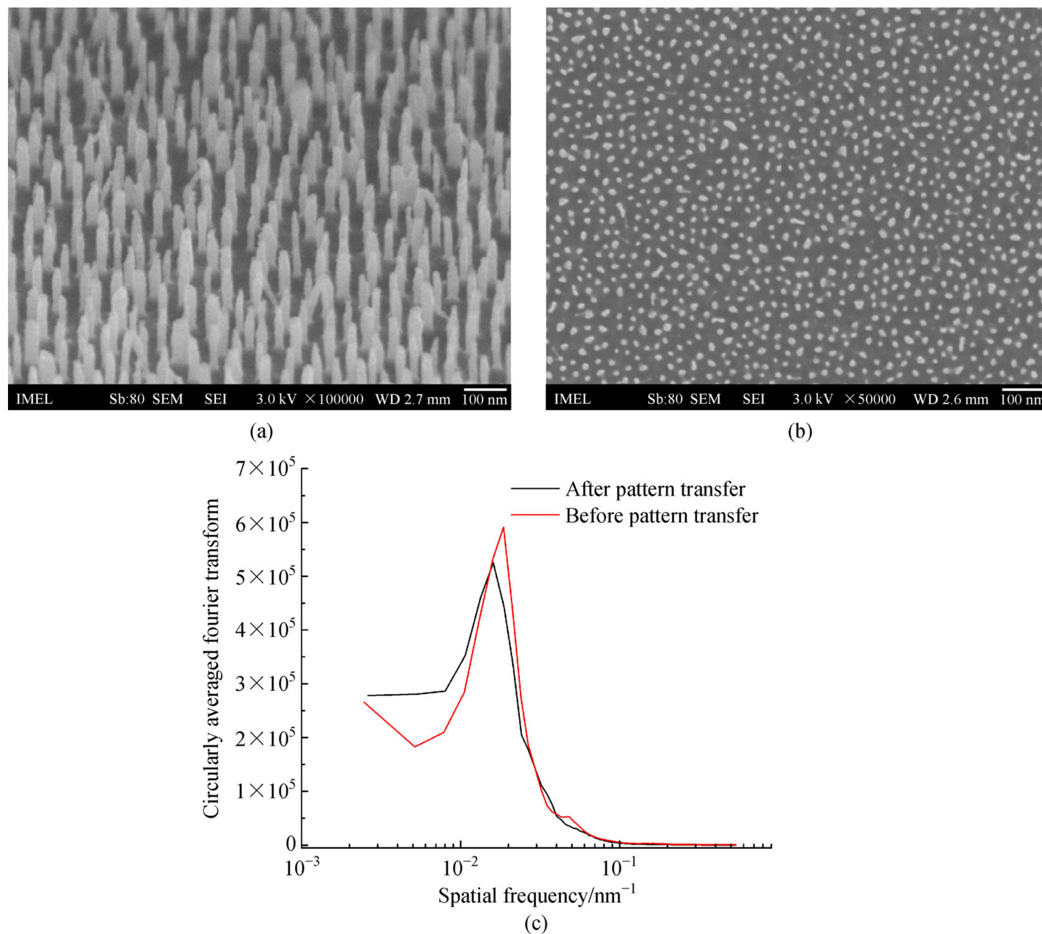

Fig. 5 (a) Tilted at 45° and (b) top-down SEM images of silicon nanopillars as a result of plasma etching (room-temperature mixed process) using as a mask for the PMMA nanodots; (c) Circularly average Fourier Transform of the PMMA nanodots before pattern transfer (red line) and the Si nanopillars resulting after pattern transfer (black line), obtained by SEM image analysis using the nano-TOPO-SEM™ software. The observed peak indicates the order of the nanostructures

~3.5 μm at 120 s of etching. Due to the high etch rate of the cryogenic process, combined with the much higher selectivity over the PMMA mask compared to the room-temperature mixed process, the result of the pattern transfer is the formation of high aspect ratio nanotip or nanocone-like structures which are not ordered, but show extremely low reflectance, as it can be identified by naked eyes from its characteristic black color. Figure 6(c) shows a SEM image of the reference sample surface, where bare Si is etched for 85 s. We see that there is no nanostructuring on the surface (absence of “black silicon” formation) meaning that nanostructuring showed in Fig. 6(b) is only due to pattern transfer from the PMMA nanodots.

Figure 6(d) presents the weighted total, specular and diffuse reflectance of the nanostructured silicon surfaces as a function of the pattern transfer cryogenic etching time (25, 40, 60, 85, and 120 s). The corresponding reflectance of the untreated polished silicon wafer are also shown. We observe that reflectance (both specular and diffuse) decreases when etching time, and thus the height of the nanostructuring, increases. Total weighted reflectance is 17.08% for the 25 s of etching and decreases to below 5% for etching times longer than 60 s. The minimum total reflectance is 2.26% for 120 s; specular weighted reflectance decreases to 0.88%. Light diffusion is strong and surpasses the specular reflectance for etching times higher than 60 s. The use of the PMMA nanodots pattern gives full control on the formation of the Si nanocone or nanotips-like structures. The height of the nanostructures can be easily tuned by varying the etching time. This gives also a control on the optical properties, as the optical response in terms of reflectance of the surfaces can be tuned at will, for their use in possible applications.

4 Conclusions

In this paper, we have demonstrated the fabrication of quasi-ordered, well-defined PMMA nanodots with a diameter of 25 nm using the non-lithographic process of plasma nanoassembly. These nanodots are ideal to serve as etching mask to transfer the pattern to the subsequent

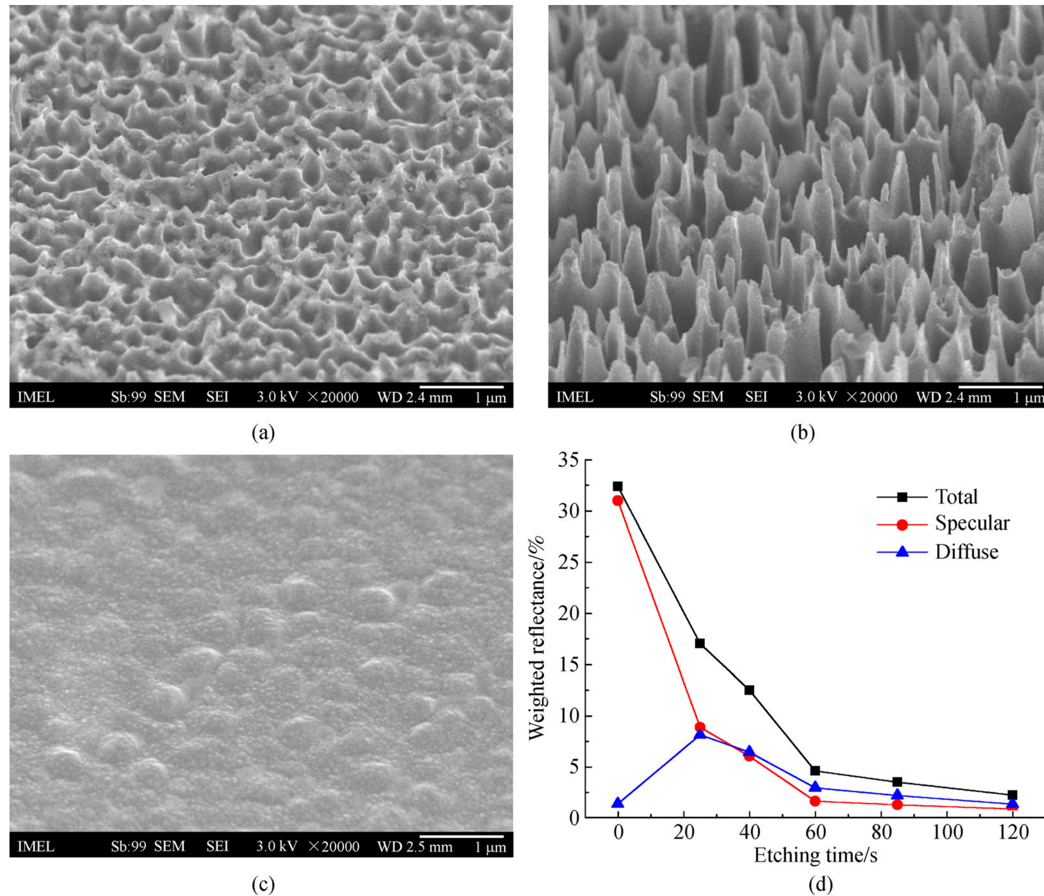

Fig. 6 (a–b) SEM images (tilted 70°) of silicon surfaces after cryogenic plasma etching for 25 s and 85 s, respectively, having the PMMA nanodots as etching mask; (c) SEM images (tilted 70°) of silicon surface after 85 s of cryogenic plasma etching an o bare surface without nanopattering (reference sample); (d) Weighted reflectance (total, specular and diffuse) of nanostructured Si surfaces by the cryogenic plasma process (etching time from 25 to 120 s) having as mask pattern the plasma directed assembly PMMA nanodots. The weighted reflectance of a polished silicon wafer (t = 0 s) is also plotted as a reference

silicon wafer. By using a custom made shield on the clamping ring of the electrode, sputtering of etch inhibitors from inside the plasma reactor can be controlled. ToF-SIMS measurements confirmed the elimination of sputtered alumina inhibitors on the surface of the etched samples. As a result, the size and shape of the nanodots can be controlled by varying bias power or etching time. By using these nanodots as etching mask and a mixed fluorine-fluorocarbon-oxygen nanoscale etch process, we have also demonstrated the fabrication of quasi-ordered silicon nanopillars with a diameter of 25 nm and an aspect ratio of 5.6. Moreover, using the cryogenic plasma process, we have successfully fabricated high aspect ratio Si nanotip or nanocone-like features that exhibit adjustable antireflective properties with a minimum total weighted reflectance of 2.26% and a specular weighed reflectance of 0.88%.

Acknowledgements The authors would like to thank Dr. Dimitrios Kontziampasis for his contribution in the AFM measurements and his important work on the development of the plasma directed assembly process. This work was supported by (a) the Research Excellence Project ‘Plasma Directed Assembly and Organization—PlasmaNanoFactory’ which is implemented under the ‘Aristeia I’ Action of the ‘Operational Programme Education and Lifelong Learning’ (Project ID 695) and is co-funded by the European Social Fund (ESF) and National Resources, (b) the Ph.D. fellowship programme of NCSR Demokritos which supported Dr. A. Smyrnakis, and (c) the M. Smoluchowski Krakow Research Consortium (in the framework of the KNOW project).

References

1. Gogolides E, Vassilios C, George K, Dimitrios K, Katerina T, George B, Marilena V, Angeliki T. Controlling roughness: From etching to nanotexturing and plasma-directed organization on organic and inorganic materials. Journal of Physics. D, Applied Physics, 2011, 44(17): 174021
2. Franssila S. Optical Lithography. Introduction to Microfabrication. Hoboken: John Wiley & Sons, Ltd., 2010, 103–113
3. Stulen R H, Sweeney D W. Extreme ultraviolet lithography. IEEE Journal of Quantum Electronics, 1999, 35(5): 694–699
4. Pfeiffer H C. Direct write electron beam lithography: A historical

overview. In: Proceedings of SPIE Photomask Technology. Monterey: SPIE, 2010, 782316
5. Chou S Y, Krauss P R, Renstrom P J. Nanoimprint lithography. Journal of Vacuum Science & Technology. B, 1996, 14(6): 4129–4133
6. Schift H. Nanoimprint lithography: An old story in modern times? A review. Journal of Vacuum Science & Technology. B, 2008, 26(2): 458
7. Colson P, Henrist C, Cloots R. Nanosphere lithography: A powerful method for the controlled manufacturing of nanomaterials. Journal of Nanomaterials, 2013, 2013: 1–19
8. Zhang G, Wang D. Colloidal lithography—the art of nanochemical patterning. Chemistry, an Asian Journal, 2009, 4(2): 236–245
9. Haynes C, Van Duyne P. Nanosphere lithography: A versatile nanofabrication tool for studies of size-dependent nanoparticle optics. Journal of Physical Chemistry B, 2001, 105: 5599–5611
10. Hamley I W. Nanostructure fabrication using block copolymers—Review. Nanotechnology, 2003, 14: 16
11. Tallegas S, Baron T, Gay G, Aggrafeil C, Salhi B, Chevolleau T, Cunge G, Bsiesy A, Tiron R, Chevalier X, et al. Block copolymer technology applied to nanoelectronics. Physica Status Solidi. C, Current Topics in Solid State Physics, 2013, 10(9): 1195–1206
12. Seeger K, Palmer R E. Fabrication of silicon cones and pillars using rough metal films as plasma etching masks. Applied Physics Letters, 1999, 74(11): 1627–1629
13. Ostrikov K. Plasma nanoscience: From nature's mastery to deterministic plasma-aided nanofabrication. IEEE Transactions on Plasma Science, 2007, 35(2): 127–136
14. Levchenko I, Ostrikov K, Diwan K, Winkler K, Mariotti D. Plasma-driven self-organization of Ni nanodot arrays on Si(100). Applied Physics Letters, 2008, 93(18): 183102
15. Hsu C H, Lo H C, Chen C F, Wu C T, Hwang J S, Das D, Tsai J, Chen L C, Chen K H. Generally applicable self-masked dry etching technique for nanotip array fabrication. Nano Letters, 2004, 4(3): 471–475
16. Gharghi M, Sivoththaman S. Formation of nanoscale columnar structures in silicon by a maskless reactive ion etching process. Journal of Vacuum Science & Technology. A, Vacuum, Surfaces, and Films, 2006, 24(3): 723
17. Muñoz-García J, Vázquez L, Castro M, Gago R, Redondo-Cubero A, Moreno-Barrado A, Cuerno R. Self-organized nanopatterning of silicon surfaces by ion beam sputtering. Materials Science and Engineering R Reports, 2014, 86: 1–44
18. Gago R, Vázquez L, Plantevin O, Metzger T H, Muñoz-García J, Cuerno R, Castro M. Order enhancement and coarsening of self-organized silicon nanodot patterns induced by ion-beam sputtering. Applied Physics Letters, 2006, 89(23): 233101
19. Frost F, Ziberi B, Schindler A, Rauschenbach B. Surface engineering with ion beams: From self-organized nanostructures to ultra-smooth surfaces. Applied Physics. A, Materials Science & Processing, 2008, 91(4): 551–559
20. Vourdas N, Kontziampasis D, Kokkoris G, Constantoudis V, Goodyear A, Tserepi A, Cooke M, Gogolides E. Plasma directed assembly and organization: Bottom-up nanopatterning using top-down technology. Nanotechnology, 2010, 21(8): 85302
21. Gogolides E, Tserepi A, Constandoudis V, Vourdas N, Boulousis G, Vlachopoulou M E, Tsougeni K, Kontziampasis D. Method for the fabrication of periodic structures on polymers using plasma processes. European Patent, EP2300214, 2009-12-17
22. Kontziampasis D, Constantoudis V, Gogolides E. Plasma directed organization of nanodots on polymers: Effects of polymer type and etching time on morphology and order. Plasma Processes and Polymers, 2012, 9(9): 866–872
23. Kokkoris G, Gogolides E. The potential of ion-driven etching with simultaneous deposition of impurities for inducing periodic dots on surfaces. Journal of Physics. D, Applied Physics, 2012, 45(16): 165204
24. Kokkoris G. Towards control of plasma-induced surface roughness: Simultaneous to plasma etching deposition. European Physical Journal Applied Physics, 2011, 56(2): 24012
25. Gogolides E, Zeniou A. Variable Faraday shield for a substrate holder, a clamping ring, or an electrode, or their combination in a plasma reactor. European Patent, EP3261111, 2017-04-26
26. Vijaya-Kumar M K, Constantoudis V, Gogolides E, Pret A V, Gronheid R. Contact edge roughness metrology in nanostructures: Frequency analysis and variations. Microelectronic Engineering, 2012, 90: 126–130
27. Kokkoris G, Vourdas N, Gogolides E. Plasma etching and roughening of thin polymeric films: A fast, accurate, *in situ* method of surface roughness measurement. Plasma Processes and Polymers, 2008, 5(9): 825–833
28. Dussart R, Tillocher T, Lefaucheux P, Boufnichel M. Plasma cryogenic etching of silicon: From the early days to today's advanced technologies. Journal of Physics. D, Applied Physics, 2014, 47(12): 123001
29. Smyrnakis A, Almpanis E, Constantoudis V, Papanikolaou N, Gogolides E. Optical properties of high aspect ratio plasma etched silicon nanowires: Fabrication-induced variability dramatically reduces reflectance. Nanotechnology, 2015, 26(8): 085301
30. Ellinas K, Smyrnakis A, Malainou A, Tserepi A, Gogolides E. "Mesh-assisted" colloidal lithography and plasma etching: A route to large-area, uniform, ordered nano-pillar and nanopost fabrication on versatile substrates. Microelectronic Engineering, 2011, 88(8): 2547–2551
31. Jansen H V. The black silicon method II. Microelectronic Engineering, 1995, 27: 475–480
32. Jansen H V. Black silicon method. VIII. A study of the performance of etching silicon using SF_6-O_2-based chemistry with cryogenical wafer cooling and a high density ICP source. Microelectronics Journal, 2001, 32: 769–777